Available online at www.sciencedirect.com
SCIENCE DIRECT®
C. R. Chimie 7 (2004) 417–424
COMPTES RENDUS CHIMIE

Preliminary communication / Communication

Geometrical description of echoes and macroscopic reorientation of samples in solid-state NMR

Christian Bonhomme *, Thierry Azaïs

Laboratoire de chimie de la matière condensée, UMR 7574, université Pierre-et-Marie-Curie, 4, place Jussieu, 75252 Paris cedex 05, France

Received 2 June 2003; accepted 23 December 2003

Available online 9 April 2004

Abstract

A geometrical approach of the quadrupolar interaction is presented. First- and second-order effects on all transitions are represented by quadrics and quartics. This approach allows a simple and exhaustive description of the Solomon multiple echoes: the *location* of the echoes in the time domain, as well as their *nature*, is determined without calculation. Experimental evidence of multiple echoes in the case of a ^{27}Al–O–P cluster is presented. The selection of 2Q coherences by appropriate phase cycling is presented as well. DAS and MQ MAS experiments are also described in this particular frame. ***To cite this article: C. Bonhomme et al., C. R. Chimie 7 (2004).***

Résumé

Une approche géométrique de l'interaction quadripolaire est présentée. Les effets de cette interaction au premier et au deuxième ordre en perturbation sont représentés par des quadriques et des quartiques. Cette approche permet une interprétation simple et complète des échos multiples de Solomon : la *position* des échos dans le domaine temporel ainsi que leur *nature* sont déterminées. Nous présentons la mise en évidence expérimentale de ces échos multiples dans le cas d'un cluster de type ^{27}Al–O–P. La sélection des cohérences à 2Q par un cyclage de phase approprié est abordée. Les expériences de réorientation DAS et MQ MAS sont illustrées. ***Pour citer cet article : C. Bonhomme et al., C. R. Chimie 7 (2004).***

Keywords: Quadrupolar nuclei; Quadrics and quartics; Solomon multiple echoes

Mots clés : Noyaux quadripolaires ; Quadriques et quartiques ; Échos multiples de Solomon

1. Introduction

Since their discovery by Hahn [1], echoes play a crucial role in the development of new experimental schemes in NMR. Solomon [2] extended the two-pulse sequence to the study of quadrupolar nuclei and observed multiple echoes for K^{127}I ($I = 5/2$). More recently, there has been a renewal of interest for quadrupolar echoes ($I = n/2$, $n \geq 3$) in static experiments, emphasizing (under precise assumptions) the location of echoes in the time domain and their nature [3–6].

* Corresponding author.
E-mail address: bonhomme@ccr.jussieu.fr (C. Bonhomme).

doi:10.1016/j.crci.2003.12.014

Moreover, two experimental schemes designed for the total averaging of the second-order quadrupolar broadening are based on echoes: the Dynamic Angle Spinning (DAS) experiment [7], and the Multiple Quantum Magic Angle Spinning (MQ MAS) experiment [8]. In both cases, the echoes are obtained under macroscopic reorientation of the sample and are encoded by isotropic components. In that sense, both schemes lead to highly resolved spectra for quadrupolar nuclei.

In this paper, we present a pictorial representation of the various transitions (single quantum (SQ), or multiple quantum (MQ)) involved in the multilevel system of a given quadrupolar nucleus ($I = n/2$, $n \geq 3$) (section 2). This approach is an extension of the ellipsoid representation [9] to higher orders of perturbation [10,11]. In section 4, we present a pictorial approach of the so-called Solomon echoes [2,5]: the location of the echoes as well as their nature (SQ and/or MQ – allowed or forbidden) will be derived very easily. The experimental evidence of Solomon echoes for an aluminophosphate cluster (^{27}Al, I = 5/2) [12] will be presented subsequently. In section 4, the DAS and MQ MAS experiments will be illustrated by *averaged* surfaces. The equations of these averaged surfaces can be derived analytically under fast rotation. The main results concerning DAS and MQ MAS (isotropic shifts...) will be easily derived. We note that our approach is essentially Cartesian and that explicit reference to the Legendre polynomials is not necessary. Moreover, we believe that such a representation may unify the notion of echo in both static and rotating modes.

2. Pictorial representation of transitions for a quadrupolar nucleus $I = n/2$ ($n \geq 3$)

Following Man [13,14], we define the line shift in Σ^{obs} (see below) related to the transition between two energy levels $|m'\rangle$ and $|m\rangle$ by:

$$\omega^{static}_{m',m} = \left\langle m' \left| \left(H_Q^{(1)} + H_Q^{(2)} \right) \right| m' \right\rangle - \left\langle m \left| \left(H_Q^{(1)} + H_Q^{(2)} \right) \right| m \right\rangle = \omega^{(1)static}_{m',m} + \omega^{(2)static}_{m',m} \quad (1)$$

Σ^{obs} corresponds to the frame rotating with the angular frequency ω_0 relative to the laboratory frame Σ^{lab}. In Eq. (1), $H_Q^{(1)}$ and $H_Q^{(2)}$ correspond to the first-order and the second-order term of the quadrupolar Hamiltonian in standard perturbation theory, respectively [15]. When $m' = m - 1$, the SQ transitions are described. $m = 1/2$ corresponds to the central transition (CT), which is not shifted by the first-order quadrupolar interaction. $m \neq 1/2$ corresponds to the ($2I$ - 1) satellite transitions (ST). When $m' \neq m - 1$, the MQ transitions are described. Assuming $\eta_Q = 0$ for simplicity, the terms $\omega_{m',m}^{(1)static}$ and $\omega_{m',m}^{(2)static}$ in Eq. (1) are given by [11]:

$$\omega^{(1)static}_{m',m} = 2\pi \frac{3}{4} \frac{C_Q}{2I(2I-1)} (3\cos^2\beta_0 - 1)(m'^2 - m^2) \quad (2)$$

$$\omega^{(2)static}_{m',m} = \frac{4\pi^2}{12\omega_0} \left(\frac{3C_Q}{2I(2I-1)} \right)^2 \left\{ \begin{array}{l} \cos^2\beta_0 (1-\cos^2\beta_0)[m(8m^2 - 4I(I+1) + 1) - m'(8m'^2 - 4I(I+1) + 1)] \\ + \frac{3}{8}(1-\cos^2\beta_0)^2 [m(-2m^2 + 2I(I+1) - 1) - m'(-2m'^2 + 2I(I+1) - 1)] \end{array} \right\} \quad (3)$$

$C_Q = e^2 q Q/h$ is the quadrupole coupling constant.

β_0 corresponds to the polar angle of $\mathbf{B}_0$ in the quadrupolar PAS (principal-axis system). In order to introduce our pictorial representation of transitions, we focus first on the first-order term, $\omega_{m',m}^{(1)static}$. Consider the quadric (second-degree surface), whose equation in the quadrupolar PAS is given by [10]:

$$(m^2 - m'^2)\left[\left(X^2 + Y^2\right) - 2Z^2 \right] = +1 \quad (4)$$

Assuming $m^2 > m'^2$, this surface corresponds to a *hyperboloid of one sheet*. The intersection of the surface with the $\mathbf{B}_0$ direction leads to the intersection radius r given by: $r^{-2} = (m^2 - m'^2)(1 - 3\cos^2\beta_0)$. It follows that $(+r^{-2})$ is directly related to the angular part of the first-order shift (Eq. (2)). For $\beta_0 < \xi_m = 54.74°$ (the magic angle), the intersection radius cannot be defined. We use then the complementary quadric, given in the PAS by:

$$\left(m^2 - m'^2\right)\left[\left(X^2 + Y^2\right) - 2Z^2 \right] = -1 \quad (5)$$

It corresponds to a *hyperboloid of two sheets*. The intersection of the complementary surface with the $\mathbf{B}_0$ direction leads to the intersection radius r given by: $r^{-2} = (m^2 - m'^2)\,(3\cos^2\beta_0 - 1)$. $(-r^{-2})$ is related to the angular part of Eq. (2).

It follows that the first-order shift, $\omega_{m',m}^{(1)\text{static}}$, corresponding to the transition between $|m'\rangle$ and $|m\rangle$, can be safely illustrated by a set of two complementary hyperboloids. *Each surface is 'signed'* (+ or –), as $(+r^{-2})$ or $(-r^{-2})$ leads alternatively to the angular part of Eq. (2). This representation can be generalized to $\eta_Q \neq 0$: two complementary *elliptic* hyperboloids are then necessary (when $\eta_Q = 0$, the corresponding surfaces are of revolution – see above). Considering the second-order shift, $\omega_{m',m}^{(2)\text{static}}$, we have shown previously that quadrics cannot be connected to the angular part of Eq. (3) [11]. However, a set of *signed* complementary homogeneous *quartics* (fourth-degree surfaces) can achieve this goal. As an example, we consider the central transition ($m' = m - 1$, $m = 1/2$), which is subjected solely to second-order effects. Eq. (3) leads to:

$$\omega_{-1/2,1/2}^{(2)\text{static}} = -\frac{4\pi^2}{6\omega_0}\left[\frac{3\,C_Q}{2\,I\,(2\,I-1)}\right]^2 \times \left[I\,(I+1) - \frac{3}{4}\right]\left[\frac{3}{8}\sin^2\beta_0\,(9\cos^2\beta_0 - 1)\right] \quad (6)$$

We define two complementary quartics in the quadrupolar PAS by:

$$(3/8)\left(X^2+Y^2\right)\left[\,8\,Z^2 - \left(X^2+Y^2\right)\right] = \pm 1 \quad (7)$$

The radius r corresponding to the intersection of the surfaces with the $\mathbf{B}_0$ direction are given by: $(\pm r^{-4}) = (3/8)\sin^2\beta_0\,(9\cos^2\beta_0 - 1)$. It corresponds exactly to the angular part of Eq. (6). At this point, several comments can be made:

- (*i*) when $\eta_Q \neq 0$, generalised quartics can always be defined; explicit Cartesian equations of these surfaces are given in [11];
- (*ii*) considering *both* terms, $\omega_{m',m}^{(1)\text{static}}$ and $\omega_{m',m}^{(2)\text{static}}$ (Eqs. (2) and (3)), the involved angular part $\text{Ang}\{\omega_{m',m}^{\text{static}}\}$ can always be illustrated by a set of complementary quartics; it follows then that $(\pm r^{-4}) = \text{Ang}\{\omega_{m',m}^{\text{static}}\}$;
- (*iii*) for any higher order of perturbation (n), homogeneous surfaces of degree $2n$ are able to illustrate the shifts, assuming $(\pm r^{-2n}) = \text{Ang}\{\omega_{m',m}^{\text{static}}\}$; for instance, sixth-degree surfaces [16] are directly connected to third-order effects on quadrupolar transitions [17].

The pictorial representations of all SQ and MQ transitions for a spin $I = 3/2$ are presented in Fig. 1.

3. Pictorial approach of Solomon echoes [2,5]

3.1. Description of evolution and refocusing of coherences by hyperboloids

The main purpose of this section is to illustrate very easily the time-domain response of a quadrupolar nucleus, subjected to a two-pulse sequence (see Fig. 2). Only *the first-order quadrupolar interaction* is considered, and dipolar couplings with other nuclei are neglected (these assumptions correspond to the quadrupolar Solomon echoes, in contrast with the so-called quadrupolar Hahn echoes [4,5,14]). The location of the various echoes in the τ_4 domain (Fig. 2), as well as their nature (SQ and/or MQ), is obtained by using the surfaces defined by Eqs. (4) and (5). As the SQ observable transitions are considered in the τ_4 period, we focus first on the ST: each ST ($m' = m - 1$) is characterised by two *signed* complementary hyperboloids (Eqs. (4) and (5)). For a given orientation β_0 of $\mathbf{B}_0$ in the quadrupolar PAS (assuming $\eta_Q = 0$ for the sake of simplicity), the shift of a particular crystallite is given by the signed intersection radius (see above). It follows that a given ST can refocus *any transition (either SQ or MQ) characterised by a set of hyperboloids of opposite signs*! We note that the CT cannot refocus evolutions occurring during τ_2, as hyperboloids cannot be defined for this particular transition ($m^2 = m'^2$).

Let us take an example: we consider the $(3,5^{-1Q})$ SQ ST ($m = 5/2$, $m' = m-1 = 3/2$, or $m^2 - m'^2 = 4$) for an $I = 5/2$ nucleus. The corresponding signed hyperboloids are shown in Fig. 2. Obviously, this SQ transition can refocus the τ_2 evolution governed by the $(-3,-1^{-1Q})$ transition ($m_1 = -1/2$, $m'_1 = -3/2$), as this transition is represented by a set of hyperboloids of opposite signs. The echo occurs at $\tau_4 = -\dfrac{m_1^2 - m'^2_1}{m^2 - m'^2}\,\tau_2 = \dfrac{\tau_2}{2}$. Considering the $(-5,1^{-3Q})$ transition ($m_2 = 1/2$, $m'_2 = -5/2$), the refocusing by the $(3,5^{-1Q})$ ST leads to an echo located at $\tau_4 = -\dfrac{m_2^2 - m'^2_2}{m^2 - m'^2}\,\tau_2 = 3/2\,\tau_2$. Our approach leads

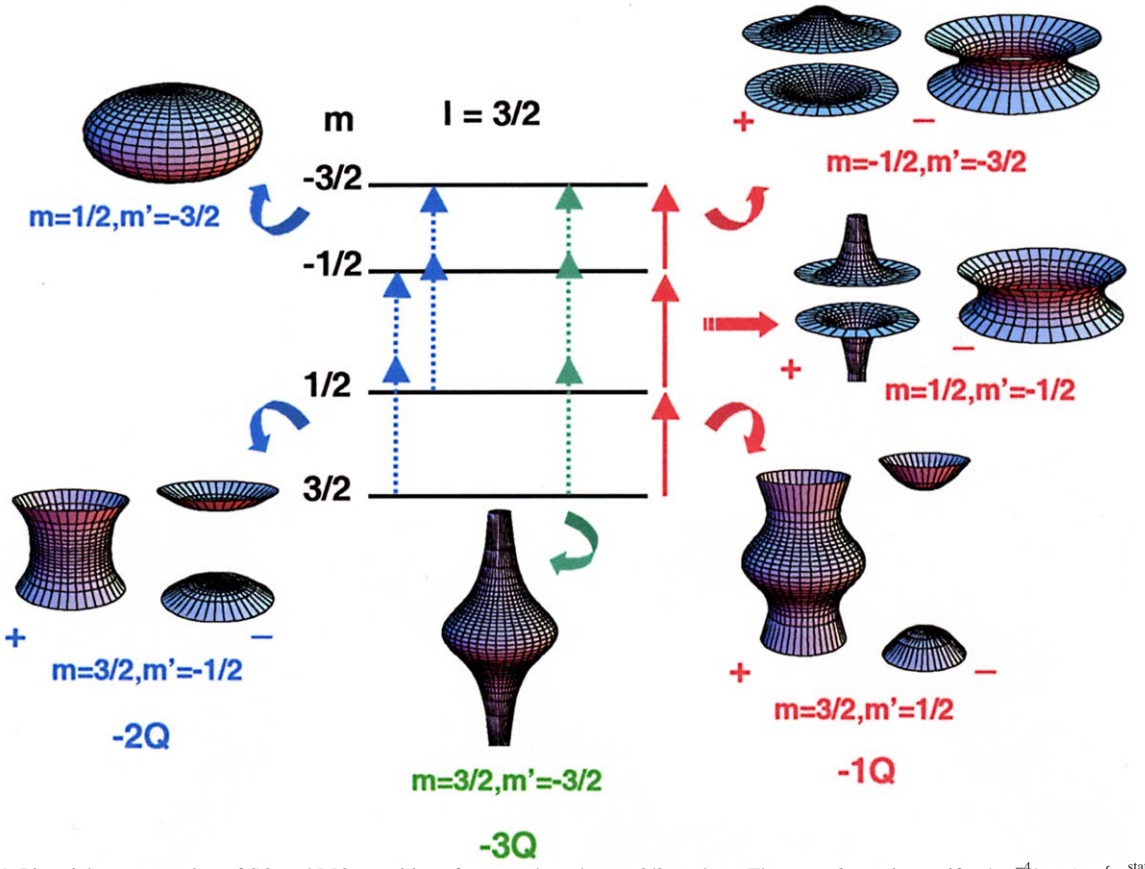

Fig. 1. Pictorial representation of SQ and MQ transitions for a quadrupolar $I = 3/2$ nucleus. The *signed* quartics verify: $(\pm r^{-4}) = \mathrm{Ang}\{\omega^{\mathrm{static}}_{m',m}\}$ (Eqs. (2) and (3)) – the ratio of the constants in Eqs. (2) and (3) is arbitrary fixed. For the CT ($m = 1/2$, $m' = -1/2$) and the –3Q transition ($m = 3/2$, $m' = -3/2$), only second-order effects are represented (as $\omega_{m',m}{}^{(1)\mathrm{static}}$ vanishes in both cases (Eq. (2)).

therefore to the exhaustive description of the contributions refocused by the $(3,5^{-1Q})$ ST: $(3,1^{1Q})$, $(3,-1^{2Q})$, $(-3,-1^{-1Q})$, $(-3,1^{-2Q})$: echo at $\tau_4 = 1/2\ \tau_2$; $(5,3^{1Q})$, $(5,-3^{4Q})$, $(-5,-3^{-1Q})$, $(-5,3^{-4Q})$: echo at $\tau_4 = \tau_2$; $(5,1^{2Q})$, $(5,-1^{3Q})$, $(-5,-1^{-2Q})$, $(-5,1^{-3Q})$: echo at $\tau_4 = 3/2\ \tau_2$. Several comments can be made:

- (*i*) using the same procedure, echoes located at $\tau_4 = \tau_2$, $2\,\tau_2$, $3\,\tau_2$ are predicted for the contributions refocused by the $(1,3^{-1Q})$ SQ ST ($m = 3/2$, $m' = m - 1 = 1/2$) (Fig. 2); the contributions refocused by the $(-3,-1^{-1Q})$ and $(-5,-3^{-1Q})$ SQ ST lead to echoes located at the same time in the τ_4 domain;
- (*ii*) the *nature* of each echo (allowed or forbidden) is easily determined by our approach; the $\tau_4 = 3/2\ \tau_2$ and $3\ \tau_2$ echoes are called 'forbidden' echoes, as they correspond to the refocusing of MQ coherences exclusively; the $\tau_4 = 1/2\ \tau_2$, τ_2 and $2\ \tau_2$ are called 'allowed' echoes; we note in particular that the $\tau_4 = 2\tau_2$ allowed echo corresponds to the refocusing of ±1Q and ±4Q coherences (see below);
- (*iii*) antiechoes, as well as transients [3,6] can also be described by the surfaces presented above; they are not represented in Fig. 2;
- (*iv*) the representation of transitions by surfaces is particularly useful for the location and description of multiple echoes involved in 3- (or more) pulse sequences [3];
- (*v*) when second-order quadrupolar effects and/or dipolar interactions are present [6], the location and nature of echoes can be adequately described by using quartics (see above) and/or hyperboloids.

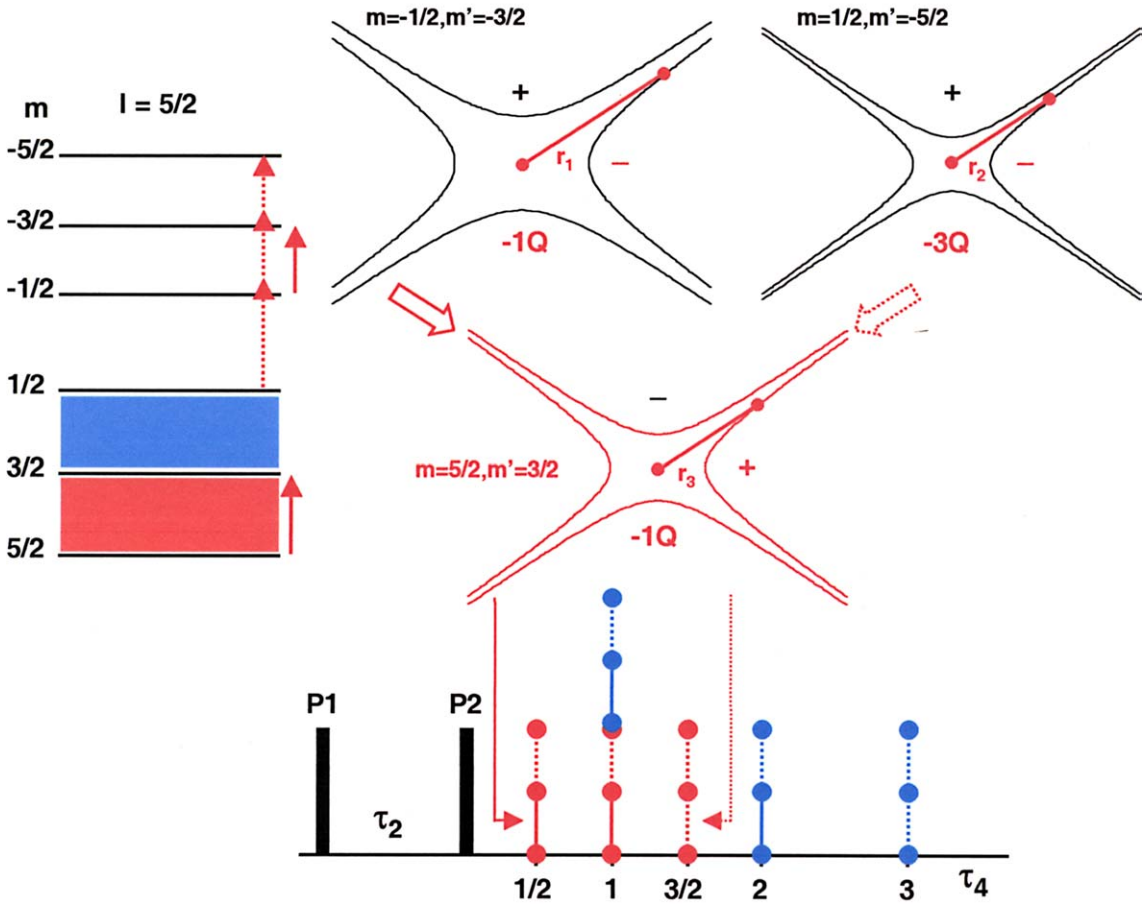

Fig. 2. Solomon echoes following a two-pulse sequence (P1, P2) ($I = 5/2$). τ_4 is given in τ_2 units. In red: refocusing of coherences by the ($3,5^{-1Q}$) SQ ST. In blue: refocusing of coherences by the ($1,3^{-1Q}$) SQ ST. Vertical solid line: refocusing of *two* ±1Q coherences. Vertical dashed-line: refocusing of *two* ±*n*Q coherences. Signed hyperboloids in red: corresponding to the ($3,5^{-1Q}$) SQ ST. Signed hyperboloids in black: corresponding to the ($-3,-1^{-1Q}$) SQ transition and to the ($-5,1^{-3Q}$) MQ transition. The contributions refocused by the ($-3,-1^{-1Q}$) SQ ST and the ($-5,-3^{-1Q}$) SQ ST are omitted for clarity.

3.2. Experimental evidence of Solomon echoes: ^{27}Al (I = 5/2)

Solomon echoes were observed very rarely. Echoes in $K^{81}Br$ ($I = 3/2$) were reported by Bonera et al. [18] and in $^{23}NaN_3$ ($I = 3/2$) by Jeffrey [19]. We note that for $I = 3/2$ one single echo at $\tau_4 = \tau_2$ is observed. Multiple echoes were observed by: (*i*) Solomon [2] in the case of $K^{127}I$ (I = 5/2), (*ii*) Sanctuary and Halstead [3] using $K^{127}I$ and two- or three pulse sequences, (*iii*) Schoep et al. [20] in a series of $^{51}V_3X$ compounds ($I = 7/2$). To the best of our knowledge, multiple echoes in the frame of ^{27}Al solid-state NMR were never reported in the literature and only mentioned once by the authors [12].

In Fig. 3a, the structure of a cubane-shaped Al–O–P cluster is presented. The synthesis and characterisation by solid-state NMR of this cluster is presented in [12] ($\delta_{iso}(^{27}Al)$ = –8.7 ppm; C_Q = 1.70 MHz; η_Q = 0.3; $\delta_{iso}(^{31}P)$ = –25.7 ppm; δ_{11} = –61.0, δ_{22} = –31.9, and δ_{33} = 15.7 ppm). Using a two-pulse sequence, multiple echoes located at $\tau_4 = \tau_2/2$, τ_2, and 2 τ_2 are clearly observed (Fig. 3b). They correspond to 'allowed' echoes. The observed echoes are superimposed to a residual FID component. Using the general concept of phase cycling [21], it is possible to select only 2Q coherences through the echo sequence. The time-domain response for the Al–O–P cubane is presented in Fig. 3c. Obviously, the FID component is remark-

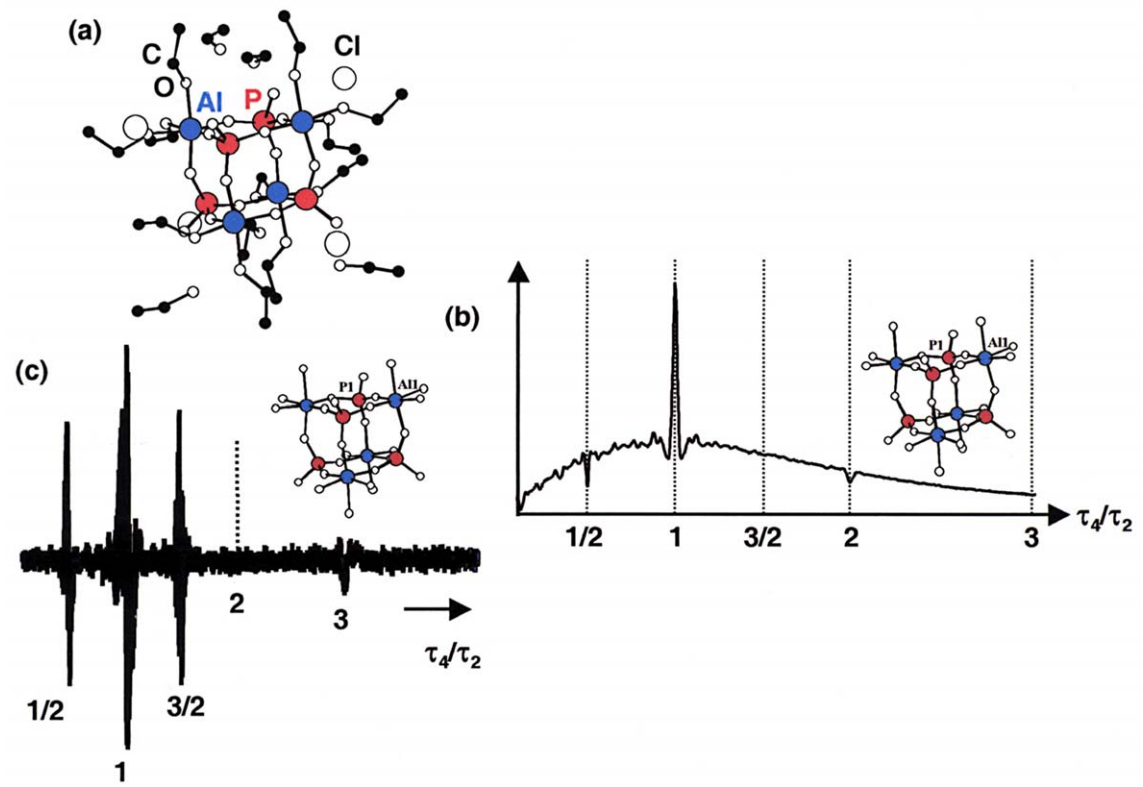

Fig. 3. (**a**) Al–O–P cubane-shaped cluster [12]. One Al1 and one P1 crystallographic sites. Al and P atoms are linked by oxo bridges. Cl^- are present as counter-anions. Al atoms are 6-fold coordinated (including three ethanol molecules as ligands). Four solvate ethanol molecules per cubane entity are present. (**b**) Solomon-'allowed' echoes located at τ_4 = 1/2, 1 and 2 τ_2. These echoes are superimposed on a FID. (**c**) Selection of 2Q coherences through phase cycling: P1, $+X+Y-X-Y$; P2, $+X+X+X+X$; Rec: $+X-X+X-X$. 'Allowed' and 'forbidden' echoes are observed. The FID is suppressed. The $\tau_4 = 2\ \tau_2$ echo is missing.

ably suppressed, leading to an improved observation of the echoes. In this case, the τ_4 = 3/2 τ_2 and 3 τ_2 'forbidden' echoes are observed. Moreover, we note that the $\tau_4 = 2\ \tau_2$ echo is not observed. Indeed, it corresponds to the refocusing of ±1Q and ±4Q coherences (see above), which are rejected by the 2Q filter.

We believe that the quantitative study of the echo amplitudes could be an interesting alternative for the structural characterisation of compounds for which the C_Q quadrupolar constants are fairly small.

4. Pictorial approach of DAS [7,22] and MQ MAS [8]

In this section, the surfaces described above (mainly quartics) will be used for the pictorial representation of macroscopic reorientations of samples in the case of DAS and MQ MAS experiments. Both schemes are 2D experiments, including a highly resolved dimension. Moreover, DAS and MQ MAS, are based on echoes under rotation, encoded with isotropic components. The 'static' quartics defined by Eqs. (3), (6), and (7) are sufficient for a *quantitative* description of the DAS and MQ MAS experiments! The key concept is to consider *averaged* surfaces, mimicking the fast reorientation of the sample: the 'static' equation is first written in a rotor frame ($X_R Y_R Z_R$), which is oriented by the Euler angles (α,β,γ) from the quadrupolar PAS [11]. Spinning the sample implies that γ becomes time-dependent. Under rapid rotation and after averaging, the quartics related to the CT (Eq. (7)) are given by (assuming $\eta_Q = 0$ for the sake of simplicity):

$$A(\beta)\left(X_R^2 + Y_R^2\right) + B(\beta)\, Z_R^4 + C(\beta)\, Z_R^2\left(X_R^2 + Y_R^2\right) = \pm 1 \tag{8}$$

with

$$A(\beta) = (3/64)\left(-27\cos^4\beta + 14\cos^2\beta + 5\right)$$
$$B(\beta) = (1/8)\left(-27\cos^4\beta + 30\cos^2\beta - 3\right) \quad (9)$$
$$C(\beta) = (3/8)\left(27\cos^4\beta - 22\cos^2\beta + 3\right)$$

(β orients Z_R in the quadrupolar PAS). These surfaces are of revolution, with Z_R as axis of revolution.

The shift under fast rotation at $\theta_1°$ (macroscopic angle) is then simply given by $(\pm r_\beta^{-4})^{\theta_1°}$ (r_β corresponds to the intersection radius of the *averaged* quartics with the $\mathbf{B}_0$ direction). It is well known that fast reorientation around a single axis is not sufficient for the total removal of quadrupolar second-order effects. The DAS experiment can be viewed as an evolution at $\theta_1°$ followed by an evolution at $\theta_2°$ during k. If high resolution is attained, the following equation must be fulfilled:

$$\left(\pm r_\beta^{-4}\right)^{\theta_1°} + k\left(\pm r_\beta\right)^{\theta_2°} = C_1 \quad (10)$$

C_1 being a constant independent of β!

Equation (10) is the direct geometrical representation of the DAS scheme. Using Eq. (9), Eq. (10) can be analytically solved, leading to the well-known DAS angle pairs [11,23]:

$$\theta_1° = \arccos\left[\frac{1}{3}\left(1 + \frac{2\sqrt{k}}{\sqrt{5}}\right)\right]^{1/2};$$
$$\theta_2° = \arccos\left[\frac{-2\sqrt{5} + 5\sqrt{k}}{15\sqrt{k}}\right]^{1/2}; \; 4/5 \le k \le 5.$$

The MQ MAS experiment can be illustrated as well. We consider first the 'static' surface corresponding to $\omega_{-3/2,3/2}^{(2)\text{static}}$ (–3Q coherence), defined by Eq. (3) (I = 3/2). The corresponding set of quartics is given by (assuming $\eta_Q = 0$ for the sake of simplicity) [11]:

$$(-3/8)\left(X^2 + Y^2\right)\left[8Z^2 + \left(X^2 + Y^2\right)\right] = \pm 1 \quad (11)$$

(see Fig. 1). Under fast rotation, the averaged surfaces are given by:

$$A_{-3}\left(X^2 + Y^2\right)^2 + B_{-3}Z^4 + C_{-3}Z^2\left(X^2 + Y^2\right) = \pm 1 \quad (12)$$

with

$$A_{-3} = (3/64)\left(21\cos^4\beta - 18\cos^2\beta - 11\right)$$
$$B_{-3} = (3/8)\left(7\cos^4\beta - 6\cos^2\beta - 1\right) \quad (13)$$
$$C_{-3} = (3/8)\left(-21\cos^4\beta + 18\cos^2\beta - 5\right)$$

Spinning around a single axis (at $\theta°$), the evolution under the MQ coherence followed by the evolution under the CT (during k) can be described geometrically by:

$$\left(\pm r_\beta^{-4}\right)_{-3/2,3/2}^{\theta°} + k\left(\pm r_\beta\right)_{-1/2,1/2}^{\theta°} = C_2 \quad (14)$$

Again, high-resolution is attained if C_2 is a constant, independent of β. Eq. (14) is fulfilled if $\theta° = \theta_m = 54.74°$ and k = 7/9; this is the MQ MAS experiment for a I = 3/2 nucleus. This approach can be extended to every value of I and every order of coherence [11].

We note the complete analogy between the DAS and the MQ MAS experiments (see Eqs. (10) and (14)). In the DAS experiment, *a single averaged* surface (CT) is involved and *two intersection radii* at $\theta_1°$ and $\theta_2°$ are necessary for the pictorial representation of the DAS echo. In the MQ MAS experiment, *two averaged* surfaces (CT and MQ) are involved and *a single intersection radius* at $\theta° = \theta_m$ is necessary for the pictorial representation of the MQ MAS echo. These results are illustrated in Fig. 4.

5. Conclusion

We have shown that the various transitions involved in the multilevel system of a quadrupolar nucleus ($I = n/2$, $n \ge 3$) can be safely illustrated by quadrics and quartics. Using quartics, it is possible to take second-order effects in account. The only prerequisite is the knowledge of the energy levels, corrected by standard second-order perturbation theory. The interpretation of Solomon multiple echoes becomes then very simple, by using sets of complementary hyperboloids. This approach becomes very efficient when more than two pulses are involved in the pulse sequence. We have also shown that the quadrupolar echoes under fast rotation of the sample can be as well illustrated by using *averaged* quartics. The *number* and *nature* of the used quartics depend mainly on the chosen experimental scheme (DAS or MQ MAS).

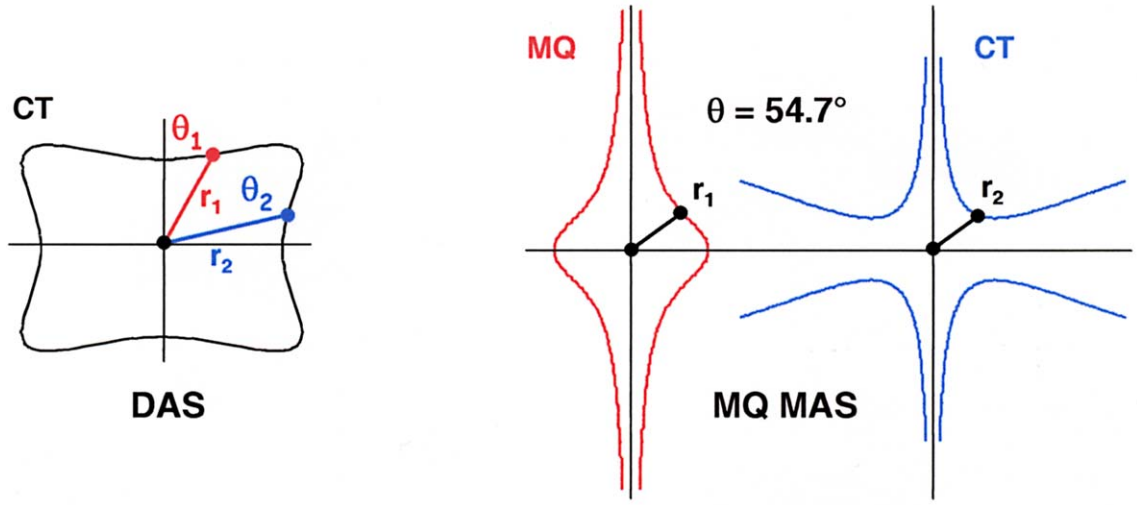

Fig. 4. Pictorial representation of DAS: the averaged CT surface is intersected at two different angles. r_1 and r_2 verify Eq. (10). Pictorial representation of MQ MAS: both averaged surfaces (CT and –3Q, $I = 3/2$) are intersected at one unique angle (the magic angle). r_1 and r_2 verify Eq. (14).

Acknowledgements

Dr. P. P. Man is warmly acknowledged for helpful discussions concerning the quadrupolar echoes.

References

[1] E.L. Hahn, Phys. Rev. 80 (1950) 580.
[2] I. Solomon, Phys. Rev. 110 (1958) 61.
[3] B.C. Sanctuary, T.K. Halstead, Advances in Magnetic and Optical Resonance, Academic Press, 1990, p. 79.
[4] P.P. Man, Phys. Rev. B 52 (1995) 9418.
[5] P.P. Man, J. Chem. Phys. 106 (1997) 3908.
[6] Y. Dumazy, J.-P. Amoureux, C. Fernandez, Mol. Phys. 90 (1997) 959.
[7] A. Llor, J. Virlet, Chem. Phys. Lett. 152 (1988) 248.
[8] L. Frydman, J.S. Harwood, J. Am. Chem. Soc. 117 (1995) 5367.
[9] J.F. Nye, Physical Properties of Crystals, Clarendon Press, Oxford, 1989 Chapter 1.
[10] C. Bonhomme, J. Livage, J. Phys. Chem. A 102 (1998) 375.
[11] C. Bonhomme, J. Livage, J. Phys. Chem. A 103 (1999) 460.
[12] T. Azaïs, C. Bonhomme, L. Bonhomme-Coury, J. Vaissermann, Y. Millot, P.P. Man, P. Bertani, J. Hirschinger, J. Livage, J. Chem. Soc., Dalton Trans. 4 (2002) 609.
[13] P.P. Man, Phys. Rev. B 55 (1997) 8406.
[14] P.P. Man, Encyclopedia of Analytical Chemistry, John Wiley & Sons, Chichester, UK, 2000, p. 12224.
[15] A. Abragam, Principles of Nuclear Magnetism, Clarendon Press, Oxford, 1989, Chapter 7.
[16] C. Bonhomme, Habilitation à Diriger des Recherches, 'Université Pierre-et-Marie-Curie', Paris, France, 2002.
[17] F. Wolf, D. Kline, H.S. Story, J. Chem. Phys. 53 (1970) 3538.
[18] G. Bonera, A. Avogadro, F. Borsa, Phys. Rev. 165 (1968) 391.
[19] K.R. Jeffrey, J. Chem. Phys. 66 (1977) 4677.
[20] G.K. Schoep, H.J.V.D. Valk, G.A.M. Fritjters, H.B. Kok, N.J. Poulis, Physica 77 (1974) 449.
[21] R.R. Ernst, G. Bodenhausen, A. Wokaun, Principles of Nuclear Magnetic Resonance in One and Two Dimensions, Clarendon Press, Oxford, 1990.
[22] B.F. Chmelka, K.T. Mueller, A. Pines, J. Stebbins, Y. Wu, J.W. Zwanziger, Nature 339 (1989) 42.
[23] B.F. Chmelka, J.W. Zwanziger, in: P. Kosfeld, B. Blümich (Eds.), NMR Basic Principles and Progress, 33, Springer Verlag, Berlin, 1994.